Journal of Applied Electrochemistry **32**: 929–936, 2002.

Study of a Li–Ni oxide mixture as a novel cathode for molten carbonate fuel cells by electrochemical impedance spectroscopy☆

M.J. ESCUDERO[1], X.R. NÓVOA[2,*], T. RODRIGO[3] and L. DAZA[1,3]
[1]*Dpto. Combustibles Fósiles, CIEMAT, Av. Complutense 22, 28040 Madrid, Spain*
[2]*Univ. de Vigo, E.T.S.E.I., Lagoas-Marcosende 9, 36200 Vigo, Spain*
[3]*Instituto de Catálisis y Petroleoquímica, CSIC, Campus Cantoblanco, 28049 Madrid, Spain*
*(*author for correspondence, e-mail: rnovoa@uvigo.es or m.escudero@ciemat.es)*

Received 22 June 2001; accepted in revised form 29 May 2002

Key words: cathode, electrochemical impedance spectroscopy (EIS), fuel cell, lithium nickel oxide, molten carbonate

Abstract

Li–Ni oxide mixtures with high lithium content are considered to be an alternative cathode material for molten carbonate fuel cells (MCFCs). The electrochemical behaviour of $Li_{0.4}Ni_{0.6}O$ samples has been investigated in a Li–K carbonate melt at 650 °C by electrochemical impedance spectroscopy as a function of immersion time and O_2 and CO_2 partial pressure. The impedance spectra have been interpreted using a transmission line model that includes contact impedance between reactive particles. The $Li_{0.4}Ni_{0.6}O$ powder particles show structural changes due to high lithium leakage and low nickel dissolution from the reactive surface to the electrolyte during the first 100 h of immersion. After this time, the structure seems to be stable. The partial pressures of O_2 and CO_2 affect the processes of oxygen reduction and Li–Ni oxide oxidation. X-ray diffraction and chemical analysis performed on samples before and after the electrochemical tests have confirmed that the lithium content decreases. SEM observations reveal a reduction in grain size after the electrochemical tests.

1. Introduction

The molten carbonate fuel cell (MCFC) is one of the most promising power generation systems for the present century owing to its high energy conversion efficiency, excellent environmental characteristics and its ability to utilize a wide variety of fuels such as hydrogen, natural gas and coal gasified gas [1]. Nickel oxide, which is usually obtained by *in situ* oxidation of porous nickel, has been the cathode material of choice since the 1970s [2]. However, short circuiting due to dissolution of NiO into the electrolyte followed by deposition as Ni metal is a crucial factor which delays MCFC commercialisation [3]. The electrochemical properties of the NiO cathode have been extensively investigated, but the reaction mechanism of oxygen reduction and the mechanism of the lithiation process remain unresolved [4–7].

Alternative materials such as $LiFeO_2$ and $LiCoO_2$ have been proposed as a substitute for NiO [8–10]. These oxides are more stable than NiO in MCFC conditions but their electrochemical performance is lower. Nevertheless $LiCoO_2$ is regarded as a promising candidate material, although it is still limited for producing large electrodes because of its brittleness and higher manufacturing cost than the Ni-based cathode [11].

Hatoh et al. [12] showed that $Li_xNi_{1-x}O$ with high lithium content ($x < 0.2$) has a relatively lower rate of dissolution than the $Li_xNi_{1-x}O$ cathode with lower lithium content ($0.02 < x < 0.05$), obtained by *in situ* oxidation/lithiation. Preliminary work [13] demonstrated that $Li_xNi_{1-x}O$ ($0.3 < x < 0.4$) prepared by *ex situ* lithiation has higher stability in molten carbonate than NiO.

On the basis of these investigations, a new cathode material, $Li_{0.4}Ni_{0.6}O$, was prepared by *ex situ* NiO lithiation in a powder sintering process. In the present work, the dissolution of $Li_{0.4}Ni_{0.6}O$ cathode and oxygen reduction have been studied by means of electrochemical impedance spectroscopy (EIS). The samples were analysed by X-ray diffraction (XRD), scanning electron microscopy (SEM), and inductively coupled plasma (ICP-AES), before and after of exposure. The principal aim of this work is to evaluate the $Li_{0.4}Ni_{0.6}O$ cathode as an alternative cathode for molten carbonate fuel cells.

☆This paper was initially presented at the 5th International Symposium on Electrochemical Impedance Spectroscopy at Marilleva, Trento, Italy, June 2001.

2. Experimental details

2.1. *Synthesis*

The samples were synthesised using a solid-state reaction. Nickel powder (99.9% Johnson Matthey) of particle size 3–7 μm and Li_2CO_3 (99%, Panreac) were used as starting materials. Ni powder was added to a Li_2CO_3 solution prepared in distilled water to 0.4 lithium atomic fraction. A homogeneous mixture was obtained using a rotating evaporator at 80 °C. Precursor samples were pressed into pellets at 20 Tm cm^{-2} for 5 min. The samples were calcined at 800 °C for 6 h.

2.2. *Electrochemical measurements*

The electrochemical characterization of the new cathode material was carried out by means of electrochemical impedance spectroscopy (EIS). The test cell was an alumina crucible contained in a covered stainless steel reactor. The cover of the reactor was adapted to hold a thermocouple, a gas inlet/outlet and two electrodes. The cell was assembled with two nominally identical electrodes. Such a configuration allows elimination of the influence of the counter electrode and avoids the use of a reference electrode that is, by itself, a noise source [14]. Gold wires inserted in the core of each sample and shielded from the electrolyte by an alumina tube sealed by ceramic cement made the electrical connection to the electrodes.

Digital mass flow controllers/meters were used to provide the desired gas mixture compositions of O_2, CO_2 and N_2. The gas mixture flowed into the melt through a long alumina tube.

The crucible was charged with 75 g of eutectic carbonate mixture (62% mol Li_2CO_3 and 38% mol K_2CO_3) and heated at the operation temperature, 650 °C, with a ramp of 3 °C min^{-1}. The electrodes were then inserted into the carbonate melt and the cell temperature was kept at 650 °C.

The cell impedance was measured with immersion time. An oxidizing gas mixture CO_2:O_2 40:10 was maintained to accelerate the dissolution of the cathode material. Periodically the influence of gas composition was studied using atmospheres varying from 10 to 70% oxygen at 20% constant carbon dioxide (balance N_2), and from 10 to 80% carbon dioxide with 10% constant oxygen content (balance N_2).

The impedance spectra were recorded with a potentiostat/galvanostat (EG&G model 263) and a lock-in amplifier (EG&G model 5216). The amplitude of the sinusoidal voltage signal for the impedance measurements was 5 mV. The measurements were performed at the open circuit potential and the frequency of the voltage signal was scanned from 100 kHz down to 100 μHz. Five points per frequency decade were measured.

The fitting procedure, based on the algorithm by Nelder and Mead [15], uses the simplex method to find the minimum of a function. For the present case, the function to minimize, χ^2, is defined as

$$\chi^2 = \sum_{i=1}^{N} \left[\left(\frac{a_{ei} - a_{ci}}{0.01|Z_{ei}|} \right)^2 + \left(\frac{b_{ei} - b_{ci}}{0.01|Z_{ei}|} \right)^2 \right] \quad (1)$$

where N is the total number of scanned frequencies; a_{ei} and b_{ei} the real and imaginary parts of the experimental impedance Z_{ei}, $|Z_{ei}|$ the experimental impedance modulus at frequency i, and a_{c_i} and b_{c_i} the corresponding real and imaginary parts of the calculated impedance at frequency i. Equation 1 implies that the experimental error is estimated as 1% of the impedance modulus and randomly distributed in the real and imaginary parts. Details of the fitting procedure are given in previous publications [16,17].

2.3. *Structural characterization and chemical analysis*

The structure of the samples was characterised before and after the electrochemical tests by scanning electron microscopy (SEM) using a Hitachi S-2500 microscope and X-ray diffraction using a SEIFERT 3000P diffractometer with a CuK_α radiation source. The porosity of the cathode prepared was measured by mercury porosimetry using a Micrometrics pore sizer (9310). The Li and Ni contents of the sample were determined by ICP-AES (Jobin Yvon, JY-48/JY-38) before and after the electrochemical tests. The dissolution of nickel in the molten carbonate after the electrochemical tests was also analysed by ICP-AES.

3. Results and discussion

The electrochemical impedance spectra for the $Li_{0.4}Ni_{0.6}O$ sample in Li–K carbonate melt at 650 °C under an oxidizing atmosphere of CO_2:O_2 (40:10) at different exposure time are depicted in Figure 1. As can be seen from the EIS Nyquist plots, two well-differentiated regions are present: below and over 1 Hz. In the high frequency region, two capacitive arcs are observed at long exposure time. The capacitive arc in the low frequency region increases with exposure time.

The dependence of the oxygen partial pressure at a constant pCO_2 of 0.2 atm is shown in Figure 2. The low frequency arc decreases as pO_2 increases, while the arcs in the high frequency region are not influenced by pO_2. Figure 3 presents the impedance spectra as a function of carbon dioxide partial pressure at a constant pO_2 of 0.1 atm. In the low frequency region, the capacitive arc increases with pCO_2. However, the arcs in the high frequency region increase only at $pCO_2 = 0.8$ atm.

The effect of introducing an inert gas (nitrogen) is shown in Figure 4. Three flow rates of nitrogen have been studied, i.e. 20, 40 and 60 ml min^{-1} with constant flow of CO_2 and O_2 at 40 ml min^{-1} and 10 ml min^{-1}, respectively. The impedance spectra are not significantly influenced by gas flow variations.

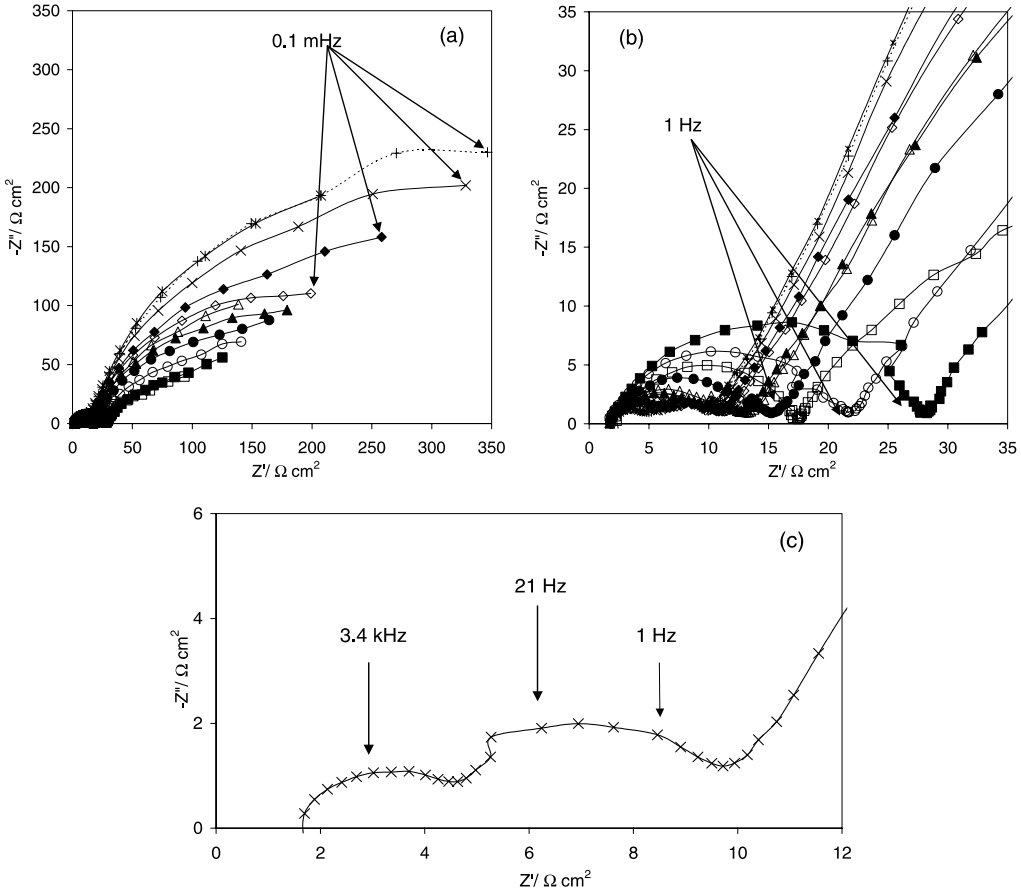

Fig. 1. Impedance spectra obtained for $Li_{0.4}Ni_{0.6}O$ samples on a two-electrode cell at the open circuit potential as a function of immersion time. (a) Low frequency region; (b) high frequency region; (c) detail of high frequency region at 246 h of immersion. Key for immersion times, *t*: (□) 6, (■) 30, (○) 54, (●) 78, (△) 102, (▲) 126, (◇) 150, (♦) 174, (×) 198, (+) 222 and (*) 246 h.

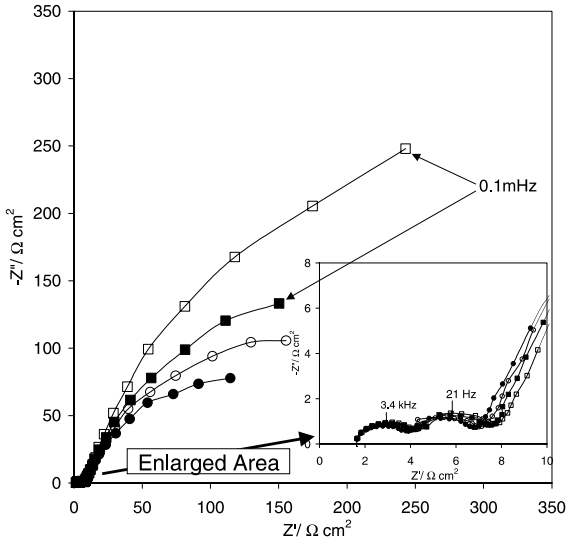

Fig. 2. Dependence of impedance spectra obtained for $Li_{0.4}Ni_{0.6}O$ on oxygen content in the feeding gas at constant 20% CO_2 content (balance N_2). *x* denotes O_2 volume fraction. Key for *x*: (□) 0.1, (■) 0.3, (○) 0.5 and (●) 0.7.

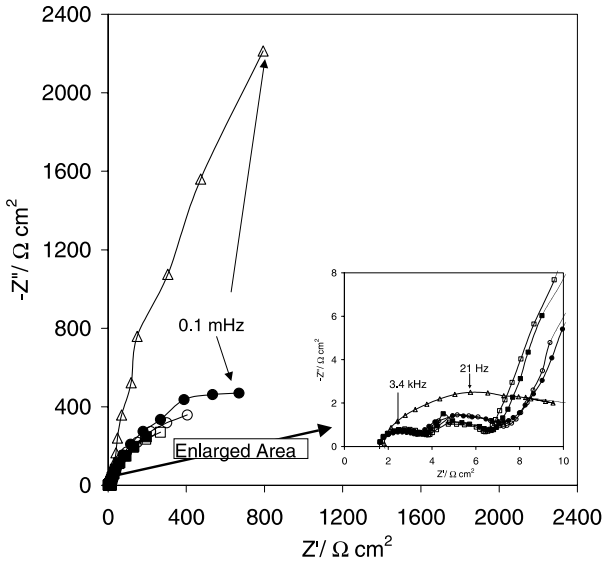

Fig. 3. Dependence of the impedance spectra obtained for $Li_{0.4}Ni_{0.6}O$ on CO_2 content in the feeding gas at constant 10% O_2 content (balance N_2). X denotes CO_2 volume fraction. Key for *x*: (□) 0.1, (■) 0.3, (○) 0.5, (●) 0.7 and (△) 0.8.

Figure 5 shows the SEM micrographs of $Li_{0.4}Ni_{0.6}O$ before and after exposure (250 h). The microstructure of the material and the reduction in grain size after testing can be seen.

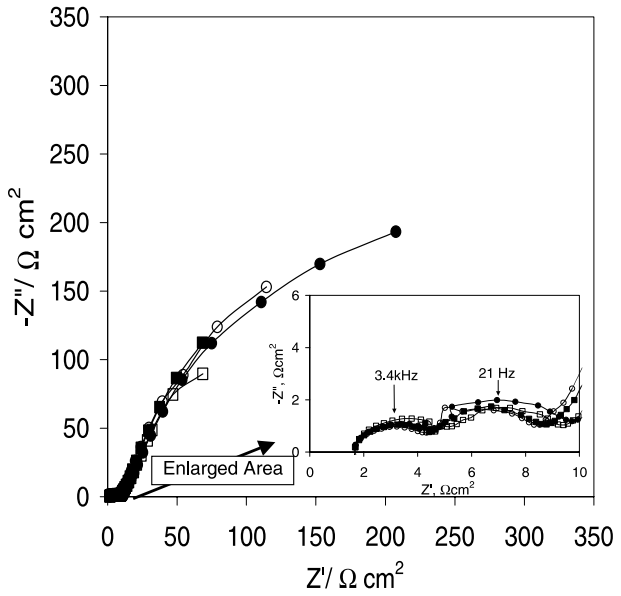

Fig. 4. Dependence of impedance spectra obtained for $Li_{0.4}Ni_{0.6}O$ on feeding gas flow rate at constant 10% O_2 and 40% CO_2. Key: (□) 20:40:10 ≡ N_2:CO_2:O_2; (■) 40:40:10 ≡ N_2:CO_2:O_2; (○) 60:40:10 ≡ N_2:CO_2:O_2; (●) 40:10 ≡ CO_2:O_2.

3.1. *Proposed model*

The interpretation of the electrochemical impedance spectra has been performed using a mathematical model based on equivalent circuits. The following assumptions were made:

(i) The sample is porous in nature; 27% porosity as measured by mercury porosimetry. Figure 5 shows the particles composing the structure as well as the pores present. This suggests the application of some kind of transmission line model involving contact impedance between particles and the redox processes taking place on each particle.

(ii) Due to the method of electrode construction, the transformations in the material takes place at the sample surface. So, the transmission line should be in series with some intrinsic impedance associated with the electrical contact between the reactive surface and the gold wire inserted into the sample, in the nonreacting core.

(iii) The oxygen reduction reaction is not a diffusion-controlled process. As observed in Figure 4, the impedance spectra do not change significantly with gas flow rate.

The sample immersed in the molten carbonate mixture suffers structural changes in its surface, so a reactive volume and an inert volume can be distinguished, as depicted in Figure 6(a). The reactive volume was assumed constant during the experiment and involving one fifth of the sample thickness (the transformed section at the end of the experiment, obtained by SEM observation of the cross section). Assuming that lithium ions migrate from the sample surface to the carbonate eutectic involving Ni^{2+} oxidation, the following transformation in solid phase can be proposed (Equation 2):

$$x\mathrm{Li_2O} + (1-x)\mathrm{NiO} \rightarrow \mathrm{Li}_x^{+}\mathrm{Ni}_x^{3+}\mathrm{Ni}_{1-x}^{2+}\mathrm{O}^{2-} + x\mathrm{Li}^{+} + x\mathrm{e}^{-} \quad (2)$$

$$\frac{1}{4}x\mathrm{O_2} + \frac{1}{2}x\mathrm{CO_2} + x\mathrm{e}^{-} \rightarrow \frac{1}{2}x\mathrm{CO_3^{2-}} \quad (3)$$

Equation 2 corresponds to the oxide mixture oxidation, which is balanced by oxygen reduction according to Equation 3. Oxide mixture oxidation occurs for each grain from the outer to the inner part.

The impedance of the $Li_{0.4}Ni_{0.6}O$ system can be described using the equivalent circuit depicted in Figure 6(b), a uniform transmission line applicable to the behaviour of zinc rich paints [16], in series with the

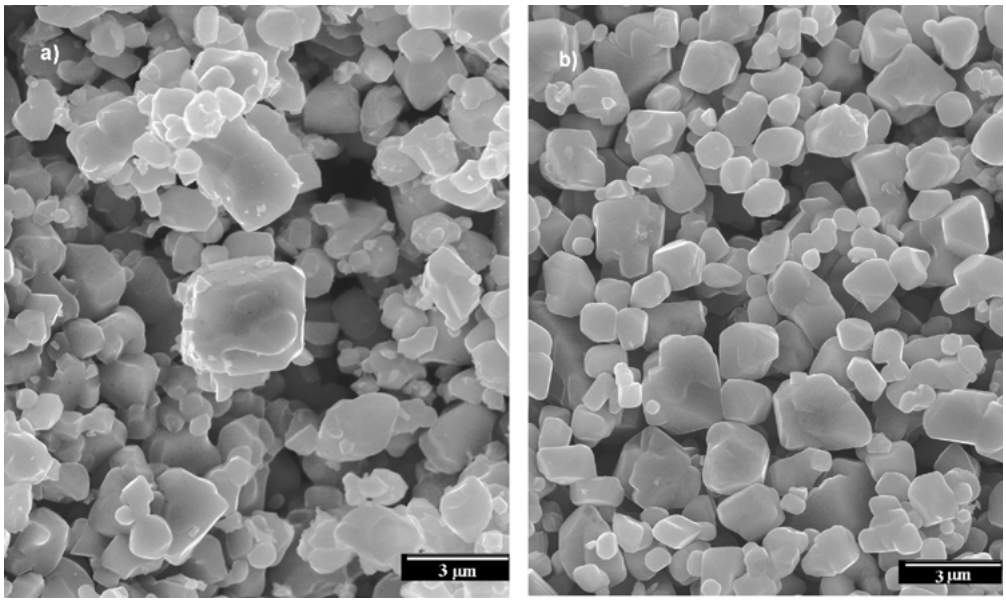

Fig. 5. SEM micrographs corresponding to the $Li_{0.4}Ni_{0.6}O$ electrode before (a) and after (b) testing.

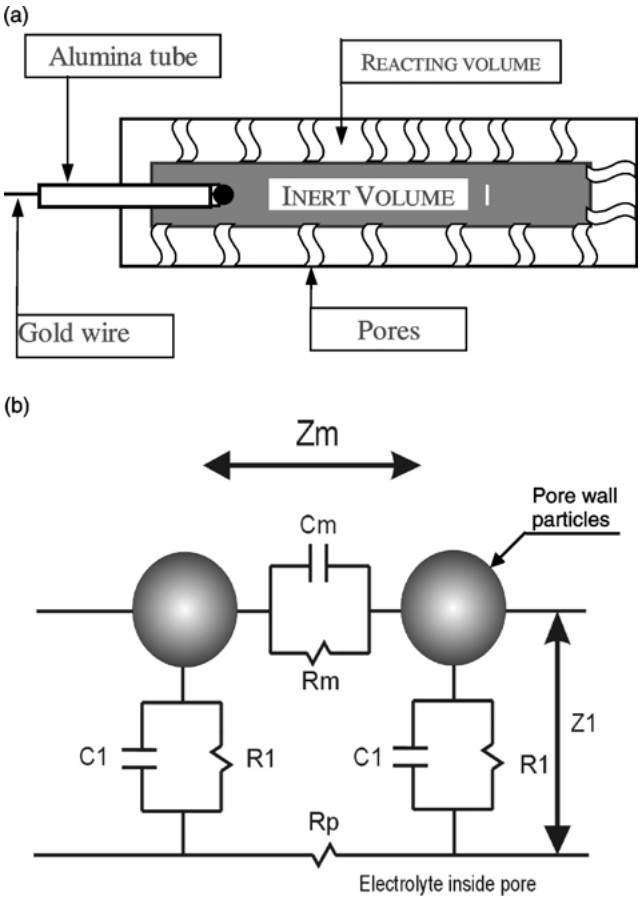

Fig. 6. Scheme of $Li_{0.4}Ni_{0.6}O$ electrode (a) and transmission line used to model its electrochemical behaviour (b).

intrinsic impedance corresponding to the inert volume and the electric contact. Thus, the overall impedance corresponds to Equation 4:

$$Z(\omega) = R_e + Z_0(\omega) + Z_{TL}(\omega) \tag{4}$$

where R_e accounts for the electrolyte resistance between both plates, and $Z_0(\omega)$ is the impedance associated to the inert volume of the electrode, including the electric contact with the gold wire. Z_{TL} represents the impedance for the reacting volume, schematically represented in Figure 6(b). The corresponding expression is Equation 5:

$$Z_{TL}(\omega) = \frac{Z_m R_p L}{Z_m + R_p} + \frac{(Z_m^2 + R_p^2)\cosh(L\sqrt{\gamma}) + 2Z_m R_p}{(Z_m + R_p)\sqrt{\gamma}\sinh(L\sqrt{\gamma})} \tag{5}$$

where L is the thickness where the structural changes take place, $\gamma = (Z_m + R_p)/Z_1$ being Z_m the contact impedance along the transmission line and Z_1 the interfacial impedance corresponding to the double layer capacitance in parallel with the charge transfer processes associated with oxygen reduction and Li–Ni oxide oxidation. R_p represents the electrolyte resistance along pores.

The intrinsic impedance, Z_0, the contact impedance, Z_m, and the interfacial impedance, Z_1, can be expressed by the following general equation for an RC parallel association (Equation 6):

$$Z_i(\omega) = \frac{R_i}{1 + (j\omega R_i C_i)_i^{\alpha}} \tag{6}$$

where the α_i parameter holds for Cole–Cole type dispersion of the R_iC_i time constant.

All impedance spectra have been fitted to Equation 4 using the procedure described in Equation 1; the results show good agreement between the experimental and fitted data. Three examples are given in Figure 7, where impedance spectra have been obtained at different gas compositions at 246 h of immersion: (a) CO_2:O_2 ratio 40:10, (b) N_2:CO_2:O_2 ratio 10:20:70 and (c) N_2:CO_2:O_2 ratio 20:70:10. The best fitting parameters are summarised in Table 1.

3.2. *Evolution of the $Li_{0.4}Ni_{0.6}O$ sample using the proposed model*

The EIS curves in Figure 1 indicate that at the beginning of immersion the sample suffers significant structural changes. The impedance results show two well-differentiated regions in the Nyquist plots. In the high frequency region, two arcs are distinguished; the first one (at highest frequencies) associated with the intrinsic impedance of the nonreacting volume, and the second one related to the impedance of particle-to-particle contact. This second arc shows important variations during the first 100 h of immersion, which can be attributed to the structural changes in the reactive surface of the electrode due to the dissolution of lithium and the oxidation of nickel. Later, the structure seems to reach a stabilized state.

The third arc, in the low frequency region, corresponds to charger-transfer processes associated with oxygen reduction and oxide oxidation. It is influenced by the immersion time and not affected by gas flow rate (Figure 4).

As can be observed in Figure 8, the structural changes are mainly related to contact impedance between the nickel particles. R_m increases with exposure time. This may be due to the particle size increasing, while the number of particles decreases, hindering contact between particles or just because oxidized particles have lower conductivity than freshly prepared ones. The last assumption will involve a constant value of the contact capacitance. As C_m decreases with immersion time (after 50 h), the first hypothesis is more likely.

The observed variation of the interfacial impedance (R_1 increases and C_1 decreases) in Figure 8 suggests a loss of reactive surface with immersion time. This may be due to the above mentioned decrease in the number of particles, or to the progress of reaction which changes particles from outside to inside, decreasing the active surface of each particle. Consequently, the charge transfer process associated with the oxide oxidation, Equation 2, slows with exposure time. The resistance of

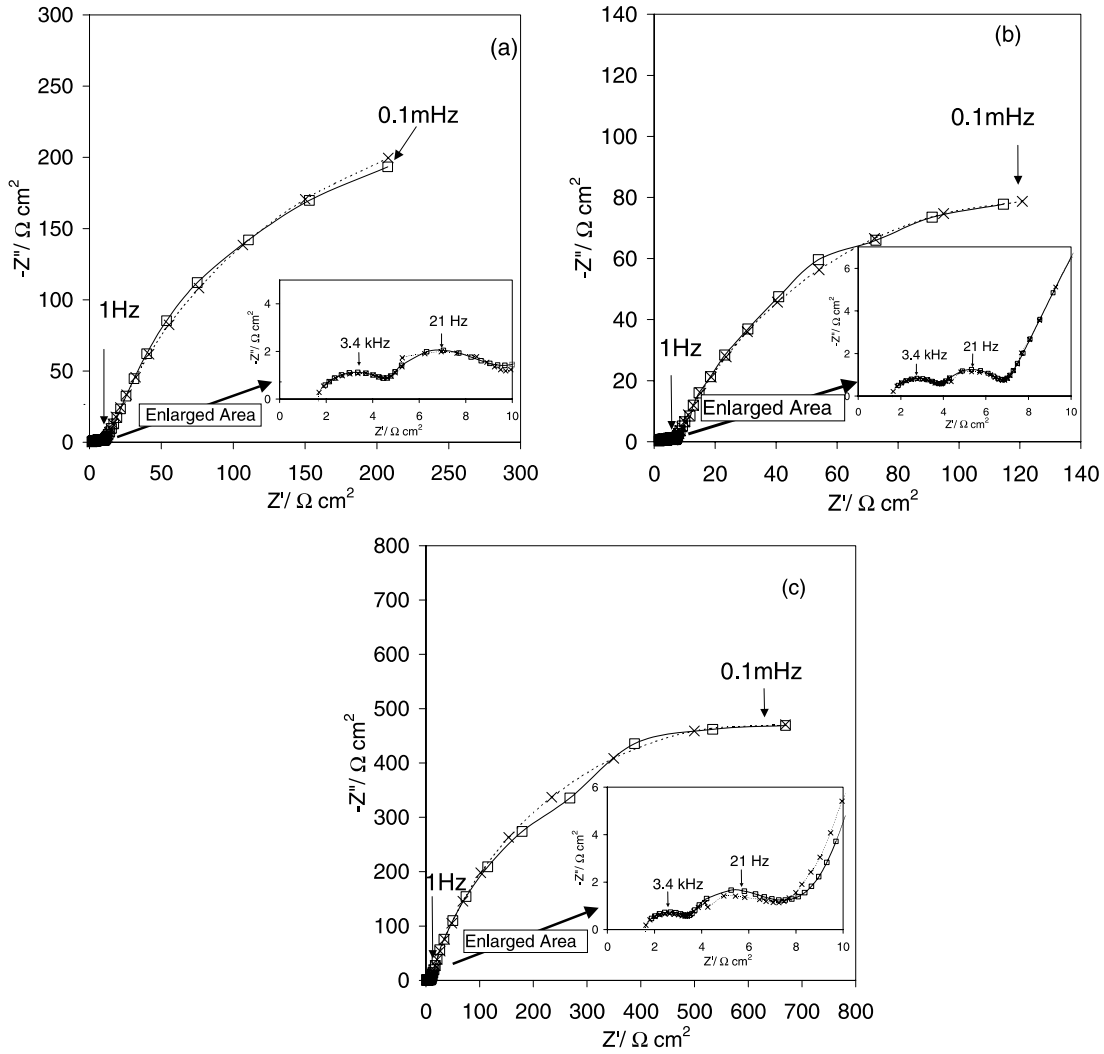

Fig. 7. Impedance spectra obtained for a $Li_{0.4}Ni_{0.6}O$ sample. Fitted values (×) have been obtained using Equation 4 as model function in Equation 1: (a) 246 h after immersion with gas volume composition CO_2:O_2 40:10; (b) with gas composition N_2:CO_2:O_2 10:20:70; (c) with gas volume composition of N_2:CO_2:O_2 20:70:10. Best fitting parameters are given in Table 1. Key: (-□-) experimental; (–×–) fitting.

Table 1. Best fitting parameters obtained using Equation 4 as model function in Equation 1 for data given in Figure 7: (a) at 246 h after immersion; (b) with gas volume composition 70% O_2, 20% CO_2 and 10% N_2; (c) with gas volume composition 10% O_2, 70% CO_2 and 20% N_2

	R_e/Ω cm^2	R_0/Ω cm^2	C_0/F cm^{-2}	α_0	R_m/Ω cm^{-1}	C_m/F cm^{-1}
Fig. 7(a)	1.52	3.21	1.82×10^{-5}	0.70	146.35	1.68×10^{-4}
Fig. 7(b)	1.48	2.31	1.90×10^{-5}	0.74	37.13	3.40×10^{-4}
Fig. 7(c)	1.54	1.82	1.95×10^{-5}	0.71	39.05	1.90×10^{-4}
	α_m	R_1/Ω cm^3	C_1/F cm^{-3}	α_1	R_p/Ω cm	L/cm
Fig. 7(a)	1	63.48	21.61	0.78	51.89	0.1
Fig. 7(b)	0.96	24.31	20.78	0.73	56.55	0.1
Fig. 7(c)	0.93	122.78	11.51	0.83	135.8	0.1

the electrolyte inside the film, R_p, increases with immersion time, which indicates pore blocking or pore length increase. This last possibility correlates well with R_0 variation, indicating displacement of the electroactive front towards the electrode core (see Figure 6(a)).

The effect of oxygen partial pressure is greater in the low frequency arc (Figure 2). As can be observed in Figure 9, R_1 decreases and C_1 remains almost constant with increasing pO_2. This suggests that oxygen reduction, Equation 3, is accelerated at constant reaction area.

As shown in Figure 3, the low frequency arc also depends on the partial pressure of CO_2 while in the high frequency region the capacitive arc increases only at a pCO_2 of 0.8 atm. As shown in Figure 10, the electrolyte resistance inside the sample, R_p and the interfacial resistance, R_1, increase from $pCO_2 = 0.3$; this can be interpreted as due to increasing difficulty of oxygen

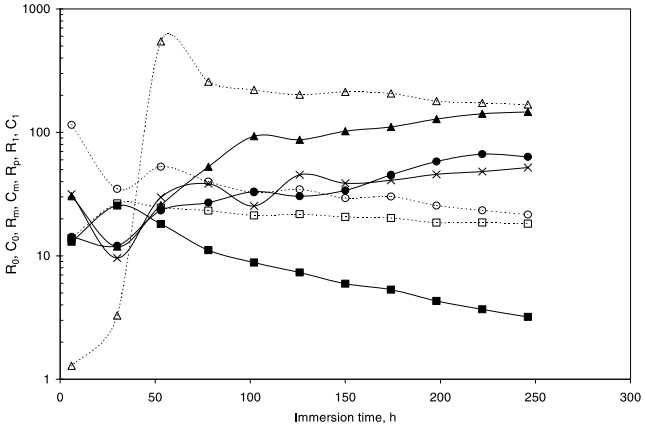

Fig. 8. Evolution of the model parameters on immersion time. Units on *y*-axis are: $R_0/\Omega\ cm^2$, $C_0/\mu F\ cm^{-2}$, $R_{m//}/\Omega$ cm, $C_m/\mu F\ cm^{-1}$, $R_{p//}$ Ω cm, $R_{1//}/\Omega\ cm^3$, $C_m/\mu F\ cm^{-3}$. Key: (■) R_o, (□) C_o, (▲) R_m, (△) C_m, (×) R_p, (●) R_1 and (○) C_1.

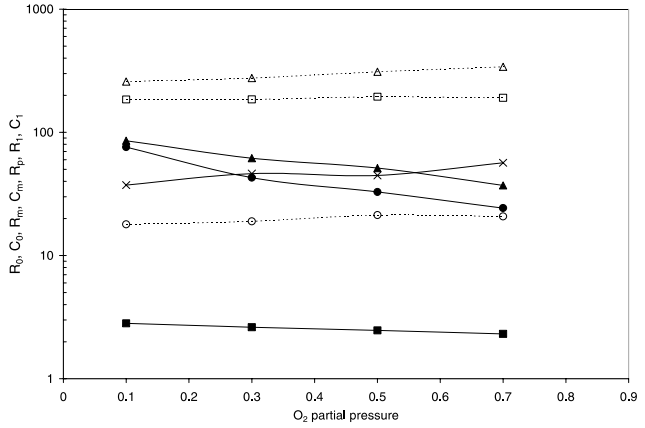

Fig. 9. Evolution of the model parameters on oxygen partial pressure at constant 20% CO_2 content (balance N_2). Units on *y*-axis are: $R_0/\Omega\ cm^2$, $C_0/\mu F\ cm^{-2}$, $R_{m//}/\Omega$ cm, $C_m/\mu F\ cm^{-1}$, $R_{p//}/\Omega$ cm, $R_{1//}/\Omega\ cm^3$, $C_m/\mu F\ cm^{-3}$. Key: (■) R_o, (□) $C_o \times 10$, (▲) R_m, (△) C_m, (×) R_p, (●) R_1 and (○) C_1.

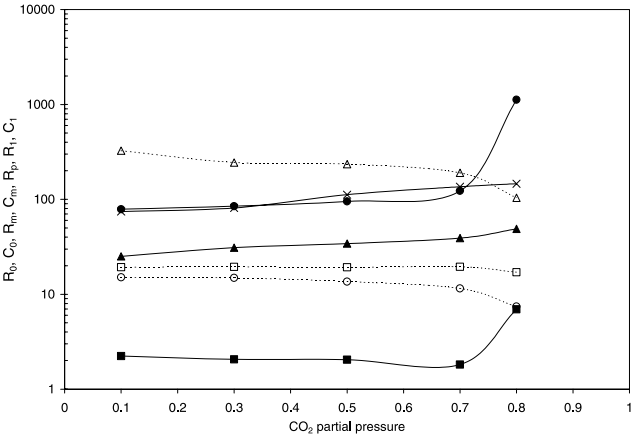

Fig. 10. Evolution of the model parameters on CO_2 partial pressure at constant 10% O_2 content (balance N_2). Units on *y*-axis are: $R_0/\Omega\ cm^2$, $C_0/\mu F\ cm^{-2}$, $R_{m//}/\Omega$ cm, $C_m/\mu F\ cm^{-1}$, $R_{p//}/\Omega$ cm, $R_{1//}/\Omega\ cm^3$, $C_m/\mu F\ cm^{-3}$. Key: (■) R_o, (□) C_o, (▲) R_m, (△) C_m, (×) R_p, (●) R_1 and (○) C_1.

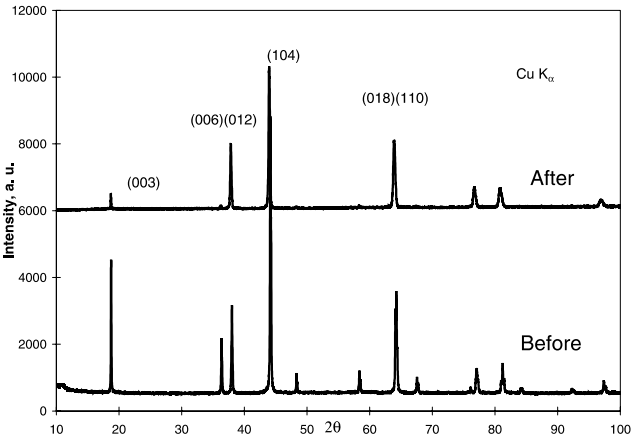

Fig. 11. XRD patterns for the $Li_{0.4}Ni_{0.6}O$ sample, before (bottom) and after (upper) testing.

transport to the reactive surface. At $pCO_2 = 0.7$, the obstruction of pores is critical, producing an exponential increase in R_1. Consequently, the oxidation process is hindered.

As expected, R_0 and C_0 values related to the non-reacting volume of the electrode remain almost constant with immersion time, O_2 partial pressure and CO_2 partial pressure (Figures 8, 9 and 10). Moreover, the electrolyte resistance, R_e (not depicted here), is not influenced by the studied variables, which may indicate a low level of nickel dissolution.

The XRD patterns of $Li_{0.4}Ni_{0.6}O$ before and after the electrochemical tests are compared in Figure 11. In both cases, the presence of peaks (003) and (104) revealed the formation of a $LiNiO_2$ rhomboedral structure. After immersion, the (003) peak shows lower intensity, this line being very sensitive to the amount of lithium. This means that the lithium content in the oxide decreases significantly indicating diffusion of lithium ions from the electrode surface to the eutectic melt.

After the electrochemical tests, the sample showed a reduction in grain size (Figure 5). Chemical analyses showed that the sample had a lithium loss of 21% and the nickel concentration in the carbonate electrolyte was 12 ppm (μg Ni per g electrolyte) after 250 h at 650 °C under an oxidizing gas mixture of CO_2:O_2 40:10. After immersion, the lithium content was 30 at %. This value is one order of magnitude higher than that estimated for *in situ* lithiated nickel oxide (1 and 4 at %) formed in molten carbonate as used as a cathode material in MCFC [18].

4. Conclusions

The impedance results have been successfully modelled using a transmission line model and show two well-differentiated regions in the Nyquist plots. In the high frequency region ($f > 1$ Hz) two arcs are present, the first being associated with electrical contact and the impedance of the nonreactive core, and the second being

related to particle-to-particle contact impedance. The third arc, in the low frequency region, corresponds to the charger-transfer processes associated with oxygen reduction and the oxide mixture oxidation. The gas composition affects the charger-transfer processes, which are accelerated by increase in pO_2 and hindered by increase in pCO_2.

The impedance spectra showed significant variations during the first 100 h of immersion. X-ray diffraction and SEM confirmed the structural and morphology changes, respectively. Moreover, chemical analysis of the sample and eutectic melt verified loss of lithium and some nickel dissolution. The lithium content in the sample at the end of the experiment was higher than the 1–4 at % reported for *in situ* formed and lithiated nickel oxide cathodes.

The stable structure after 100 h exposure indicates that the material might be used as a new cathode for MCFC, although it would be necessary to optimise the lithium content.

References

1. T. Nishina, S. Ohuchi, K. Yamada and I. Uchida, *J. Electroanal. Chem.* **408** (1996) 181.
2. B. Fang and H. Chen, *J. Electroanal. Chem.* **501** (2001) 128.
3. M. Cassir and C. Belhomme, *Plasma & Ions* **1** (1999) 3.
4. M. Mohamedi, Y. Hisamitsu, Y. Ono, T. Itoh and I. Uchida, *J. Appl. Electrochem.* **30** (2000) 1397.
5. A. Prins-Jansen, G.A.J.M. Plevier, K. Hemmes and J.H.W. de Witt, *Electrochim. Acta* **41** (1996) 1323.
6. P. Tomczyk, J. Wyrna and M. Mosialek, *J. Electroanal. Chem.* **463** (1999) 78.
7. F.J. Pérez, D. Duday, M.P. Hierro, C. Gómez, M. Romero, M.T. Casais, J.A. Alonso, M.J. Martínez and L. Daza, *J. Power Sources* **72** (2000) 309.
8. T. Fukui, H. Okawa, T. Tsunooka, *J. Power Sources* **71** (1998) 239.
9. L. Plomb, E.F. Sitters, C. Vessies and F.C. Eckes, *J. Electrochem. Soc.* **138** (1991) 629.
10. R.C. Makkus, K. Hemmes and J.H.W. de Wit, *J. Electrochem. Soc.* **141** (1994) 429.
11. T. Fukui, S. Ohara, H. Okawa, T. Hotta and M. Naito, *J. Power Sources* **86** (2000) 340.
12. K. Hatoh, J. Nikura, E. Yasumoto and T. Gamo, *Denki Kagaku* **64** (1996) 825.
13. L. Daza, M.J. Escudero, E. Hontañón, C.M. Rangel, T. Rodrigo, M.T. Casais and M.J. Martínez, 2000 Fuel Cell Seminar, Portland, Oregon, USA. Abstracts 30 Oct.–2 Nov. (2000) 732.
14. L. Giorgi, M. Carewska, S. Scaccia, E. Simoneti, E. Giacometti and R. Tulli, *Int. J. Hydrogen Energy* **21** (1996) 491.
15. J.A. Nelder and R. Mead. *Computer J.* **7** (1985) 308.
16. C.M. Abreu, M. Izquierdo, M. Keddam, X.R. Nóvoa and H. Takenouti, *Electrochim. Acta* **41** (1996) 2045.
17. M. Keddam, H. Takenouti, X.R. Nóvoa, C. Andrade and C. Alonso, *Cem. Conc. Res.* **27** (1997) 1191.
18. C. Belhomme, M. Cassir, J. Devynck and G. Gregoire, *J. Mater. Sci.* **35** (2000) 2683.